ELSEVIER

Journal of Chromatography A, 867 (2000) 71–92

JOURNAL OF CHROMATOGRAPHY A

www.elsevier.com/locate/chroma

Visualization of solute migration in chromatographic columns Quantitation of the concentration in a migrating zone

B. Scott Broyles[a,b], R. Andrew Shalliker[a,b], Georges Guiochon[a,b,*]

[a]*Department of Chemistry, The University of Tennessee, 611 Buehler Hall, Knoxville, TN 37996-1600, USA*
[b]*Chemical and Analytical Sciences Division, Oak Ridge National Laboratory, Oak Ridge, TN 37831-6120, USA*

Received 6 August 1999; accepted 12 October 1999

Abstract

The concentration distribution across a zone of iodine migrating along a column made of glass, packed with C_{18}-bonded silica, and eluted with carbon tetrachloride was derived from a quantitative analysis of the photographs of the zone. The photographs were scanned and turned into digital images. The intensity distributions obtained from the measurement of the grayscale intensity were converted into concentration profiles using a calibration method. This procedure is illustrated and suitable corrections are introduced to account for the transverse variation of the optical path length, as a result of using a cylindrical detector cell (the column itself), and for the refraction of light due to the differences between the refraction indices of the glass wall and the liquids involved. An error analysis is also reported. It shows that the method can reliably produce results with a precision of a few percent, allowing on-column evaluation of column performance and the derivation of the radial distributions of the column efficiency, the migration velocity of the zone, and the sample distribution at the head of the column.

Keywords: Visualization of solute migration; Solute migration; Instrumentation; Iodine

1. Introduction

Qualitative analysis of on-column photographs of migrating sample zones was used recently to evaluate the importance in HPLC of phenomena such as viscous fingering [1], the behavior of droplet-size zones under infinite-diameter column conditions [2], and the influence of the inlet frit on zone profiles inside the column [3,4]. This technique requires that the stationary phase and the mobile phase have matched refractive indices, and that the bed of packing material is contained within a glass column. In such a situation, colored sample zones can be viewed and photographed. The photographs can be scanned using digital imaging technologies. The distribution of photographic density across the image can be used as an approximate estimate of the distribution of the sample concentration in the zone. The technique is promising and important. Chromatographers have long wished to be able to peer inside columns, hoping to find there ready explanations for poor or unusual zone behavior. At long last, a technique allowing real-time viewing of a migrating sample zone is now feasible. It turns out, however, that while images illustrate most clearly the nature of the phenomena observed and the origin of many

*Corresponding author. Tel.: +1-423-974-0733; fax: +1-423-974-2667.
E-mail address: guiochon@utk.edu (G. Guiochon)

0021-9673/00/$ – see front matter
PII: S0021-9673(99)01085-7

sources of troubles, their multiplication does not and cannot afford quantitative results. Qualitative comparisons between different zone shapes are easy, direct quantitative ones between column performance or zone characteristics are impossible without the actual determination of the concentration distributions.

In our previous work [2], we demonstrated the process of on-column visualization of the solute migration and described the process of image collection and data analysis. However, we stopped short of using the digital images for the determination of the local concentrations across the migrating sample zones. This last step, while conceptually simple, is quantitatively demanding. The basic procedure consists in scanning the flat photograph of a cylindrical glass column. Hence, the optical path length of each light beam along which adsorption takes place and is measured varies within the sample zone across the column, decreasing with increasing distance from the column axis, and remains constant in the column direction. Furthermore, we have the equivalent of a photometric detector along each light beam. However, the measuring process involves photographic exposition and development, followed by scanning of the photographs. The behavior of the response of this complex detection mode is known to be nonlinear in a wide concentration range and a function of the film speed, the film type — color or black and white — possibly even the film lot, certainly the characteristics of the development process, and the presence and nature of filters used to assist in the detection [5]. This work addresses the issue of the derivation of quantitative concentration data in connection with on-column visualization.

2. Experimental

2.1. Chemicals

All solvents were used as supplied by their manufacturers. Reagent-grade carbon tetrachloride was purchased from Sigma (St. Louis, MO, USA). HPLC-grade dichloromethane and HPLC-grade methanol were obtained from Fisher Scientific (Fairlay, NJ, USA). Iodine (99.9%) was obtained from General Chemical Division (New York, NY, USA). The chromatographic stationary phase used was YMC 15–30 μm C_{18} chemically bonded silica (YMC, Wilmington, NC, USA).

2.2. Columns

All chromatographic experiments were performed on a 100 mm×17 mm borosilicate glass column supplied by Omnifit (Cambridge, UK).The column end fittings were prepared by the workshop of the UT Chemistry Department. Columns were slurry-packed in a downward configuration, using dichloromethane as the displacement solvent, methanol as the slurry solvent, and methanol as the packing solvent, at pressures less than 400 p.s.i. (1 p.s.i.=6894.76 Pa). (The risk of shattering the glass column or breaking its end fittings would be too high at higher pressures.) An axial compression end-fitting allows the application of a moderate but sufficient axial compression stress to the packing at the top of the bed. This ensured that no voids were present at the column inlet nor formed during normal operation. The actual bed length of the column was 6.4 cm. Visualization was improved by submersion of the cylindrical glass column into a carbon tetrachloride reservoir[1] in the form of a rectangular box with a long glass window on each of its four lateral sides. This design nearly eliminated the optical effect of cylindrical lens during the observation or photography of the column. A slight effect remains because the refraction indices of carbon tetrachloride and borosilicate glass differ slightly (see later for the quantitation of this effect).

2.3. Sample injection

Unless otherwise specified, iodine dissolved in carbon tetrachloride (12 $g\,l^{-1}$) was used as the probe solute. At this concentration, the solute zone is sufficiently colored and allows the detailed observation of the zones obtained upon the injection of the small volumes, i.e. 20 μl, used in this work, during

[1]Or a similar solvent, such as dichloromethane (see later for details).

their entire elution. Sample injection was achieved using a Rheodyne 7010 injection valve with a 20 μl loop. Iodine is not retained on C_{18} silica with CCl_4 as the eluent.

2.4. Equipment

The chromatographic system consisted of two high-performance liquid chromatographic (HPLC) pumps (model 510, Waters Associates, Milford, MA, USA) controlled by a Waters gradient profiler. A variable-wavelength UV detector (Linear) was set at 440 nm to record on-line the chromatographic response, as a conventional bulk detector. Data acquisition was obtained using a Lawson Labs Model 203 external data acquisition board and an IBM 486 personal computer.

The photographic and imaging equipment consisted of two Pentax ZX-M SLR cameras fitted one with a Promaster 100 mm fixed-focal-length macro (f 3.5), the other with a Makinon 80–200 mm macro-zoom (f 4.0) and a +4 adaptor. Hoya FL-W filters were fitted to both lenses (THK Photo Products, Rancho Dominguez, CA, USA). The film used throughout this study was Kodak 200 ASA 35 mm Ektachrome professional slide film (Kodak, Rochester, NY, USA). A Nikon Coolscan II (Nikon, Melville, New York, NY, USA) was used to scan the color slides. SigmaScan Pro 4.01 (Jandel Scientific, San Rafael, CA, USA) and Adobe Photoshop 5.0.1 (Adobe Systems, San Jose, CA, USA) were used to view and analyze the digital images. TableCurve 2D 4 (Jandel Scientific) was used for curve-fitting data, determining the best values of numerical coefficients, and generating fit statistics. A 266 MHZ Pentium II-based personal computer with 128 MB of RAM was used for the computing of the digital images and of the different scans needed.

3. Data analysis

The process of quantitating the concentration distribution throughout a migrating sample zone that is visible to the naked eye involves the following six successive steps:

- Photographing the sample zone with the two cameras located at right angles and having the photographic film developed.
- Converting the photographic image of the zone into a digital image by scanning it.
- Analyzing the digital image with the appropriate imaging software.
- Determining the detector characteristics needed: (i) the detector dynamic linear range; (ii) the maximum sample concentration compatible with a linear response; (iii) the calibration curve against a series of standards with known concentrations; and (iv) the correction to be applied as a function of the radial distance for the variable optical path length.
- Determining the possible need for a correction for the angle of refraction of light as it passes from the stationary phase–carbon tetrachloride sample cell through the glass wall and then through the viewing reservoir.
- Normalizing the local amount of analyte measured to the amount of stationary phase available in any particular section of the column.

The first three processes were previously addressed [2]. In this paper we present an evaluation of the final three steps. The following discussion is clarified by the schematics in Fig. 1 and a few definitions. The scanned image has approximately 850×3000 pixels. In order to reduce sufficiently the intensity of the noise, these pixels are bunched by groups of approximately 40×40 pixels. The optical density measured for one bunch is directly related to the light absorption experienced by the beam coming from the light source and through the column, in the direction perpendicular to the film, at the bunch (Fig. 1). The distance *OL* is the radial distance of the bunch. The optical density results from the absorption of light by the analyte over the entire length of the trajectory inside the packing material. It is a function of the product of the path length through the packing material and the average concentration or, rather, of the integral of the concentration distribution along this path length. Conversely, from the calibration, it is possible to derive the average concentration of the analyte solution along the optical path length, but this does not give any information regarding any possible variation of the concentration along the path.

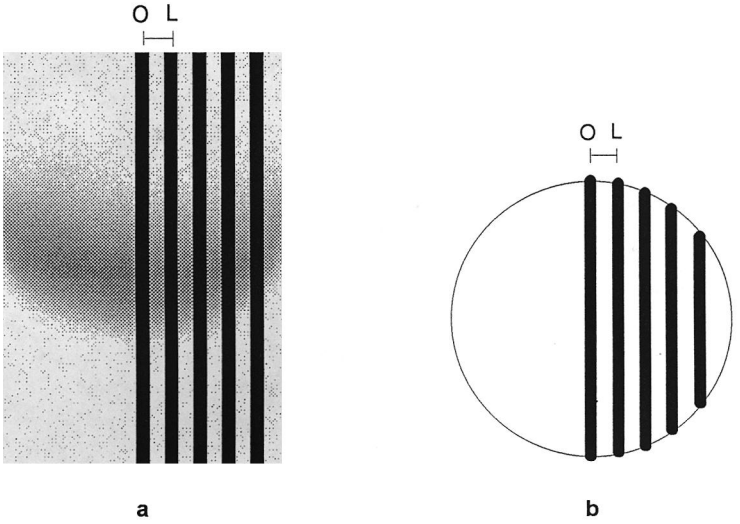

Fig. 1. Schematics of the sectioning of the column. For the sake of clarity every other section is shown on the right-hand side of the column only, beginning with the center cut. In this case cuts made at 0.2*R*, 0.4*R*, 0.6*R* and 0.8*R* are shown, where *R* is the column radius. All cuts have the same width. However, 19 sections were used for a complete analysis. (a) Overlay of the digital image of a zone and the vertical cuts of the five odd-ranked sections. (b) Cross-section of the column with the optical axis of the system and the horizontal cuts of the five odd-ranked sections.

3.1. Determination of the detector characteristics (dynamic linear range and calibration)

In our experiments, a cylindrical column behaves as an absorption cell in photometry. However, its path length decreases continuously with increasing transverse distance, *OL*, from the column center to its wall [Fig. 1(a)]. The path length is calculated as the chord length of the column cross-section in the direction of the camera axis [Fig. 1(b)]. It decreases from 17 mm at the column center to 0 mm at the column wall. Since absorption is a function of the sample concentration and the path length (Beer–Lambert Law), this path length change must be taken into account in the calibration. The obvious solution was to determine a sufficient number of calibration curves, at different transverse distances.

The procedure adopted for calibration consisted of percolating four column volumes of solutions of known concentrations of iodine through the column after recording the elution of the breakthrough curve, then photographing the column and measuring the grayscale intensity along slices parallel to the column axis [Fig. 1(a)]. However, iodine solutions in carbon tetrachloride are very corrosive and aggressive to the pump. Accordingly, all the development work needed to prepare the calibration measurements which were strictly necessary was carried out under static conditions as explained below.

To determine the extent of the linearity of the film response to the concentration of the sample or rather to the absorbance along the corresponding optical path, an empty glass column was first plugged at its bottom and filled with a homogeneous iodine solution. This column was placed in the viewing cell filled with dichloromethane (the decision to use this solvent is explained in the next section) and photographed under the same experimental conditions as the chromatographic column. This experiment was repeated with 13 iodine solutions of increasing concentrations, ranging from 0.025 g l^{-1} to 12 g l^{-1}, plus a blank solution of neat carbon tetrachloride. The images obtained were analyzed step by step, just as the sample images, using Sigmascan Pro 4.01.

Grayscale intensities, ranging from 0 (black) to 255 (white), were measured along bands parallel to the column axis [vertical bands in Fig. 1(a)], using a scan line layer width of 0.82 mm, centered at 0.1 increments of the radius (*R*), starting at the column center and moving outward on each side to 0.9*R*.

This procedure produced a total of 19 vertical bands of grayscale intensities for each concentration, each one corresponding to a particular path length and containing a homogeneously distributed sample of known concentration. Since the solution was homogeneous, the values measured for all bunches in each vertical band were averaged and the average grayscale value was assigned to that particular path length for each concentration. In all, 10 unique path lengths were defined (nine symmetrical pairs and one in the center). In a first step, the calibration curves corresponding to the 19 sections were derived from the measurements of the average grayscale intensities obtained with the column tube filled with homogeneous solutions of iodine in carbon tetrachloride at various known concentrations.

In systematic studies similar to the one reported here but carried out with different films and filters, it was found that the combination of a color slide film and an FL-D lens filter utilized in this study gave the best compromise between the different requirements. Under these conditions, the analysis of 0.025 $g\,l^{-1}$ solution showed no grayscale intensity difference from the blank solution, but a difference was observed for all the other solutions. Thus, the limit of detection (LOD) for this film and filter combination is 0.050 $g\,l^{-1}$, which was the next to lowest concentration tested. Therefore, 12 concentrations were used to construct a calibration curve for each path length measured on each side of and including the center of the column. This method produced 19 calibration curves, each containing 12 concentrations with the best-fit equation shown below:

$$C = \left(a + \frac{b}{\sqrt{I}}\right)^{-1} \quad (1)$$

where C represents the concentration of iodine in $g\,l^{-1}$, I is the grayscale intensity, and a and b are numerical coefficients. The r^2 values for these correlations are all larger than 0.997.

The data corresponding to the column center are shown in Fig. 2. A severe deviation from linear behavior is observed overall, with a rapid saturation of the response and an asymptotic limit reached at a

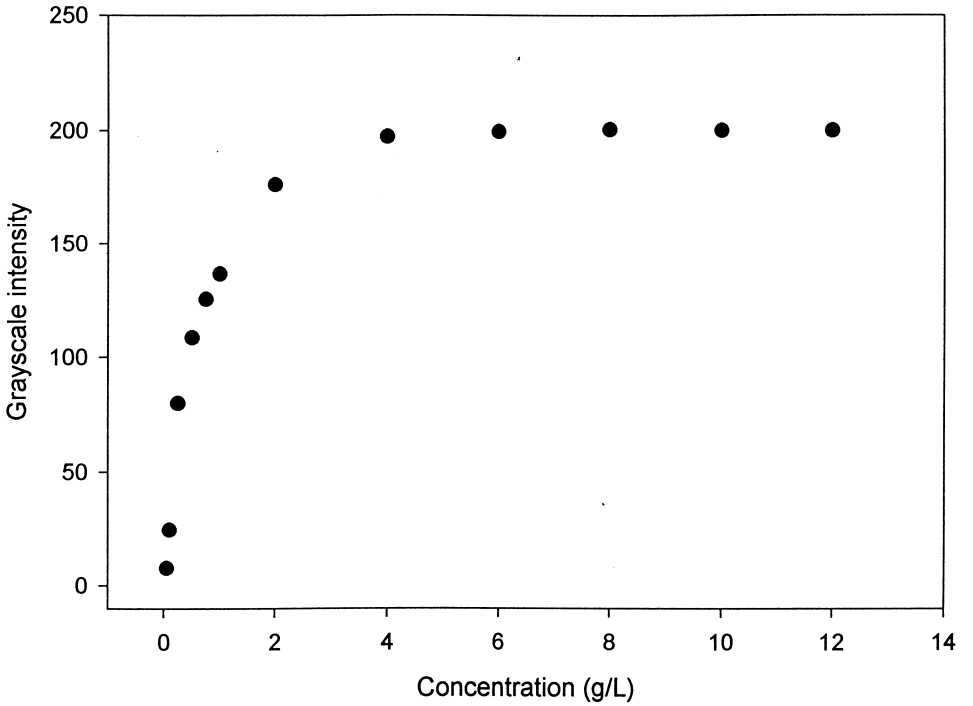

Fig. 2. Complete concentration calibration curve for iodine standards in an empty column, for the central column region, over the concentration range 0.025–12 $g\,l^{-1}$. Film: Kodak Ektachrome professional slide film 200 ASA.

concentration of 4 $g\,l^{-1}$, corresponding to a grayscale intensity of 200. Thus, the useable region of the calibration curve encompasses approximately the range 0–2 $g\,l^{-1}$.

Obviously, in a packed column the iodine does not have access to the entire column volume since a significant fraction of this volume is occupied by the solid silica and the bonded alkyl layer. As a result the effective path length at each fraction of the column radius is less than the path length in the absence of packing material. The path length decrease depends on the column porosity. Given the precision of our measurements, a few percent, and the degree of reproducibility achieved in column packing, the porosity may be considered as constant from column to column, at least for a given brand of packing material. Because the extension stress of glass is limited, the amount of stress applied to the bed was small and the packing density, and, hence the external porosity, was assumed to be constant across the bed. The volume of the empty column tube (length 6.03 cm, I.D. 17 mm) was 13.7 ml. The hold-up volume of the packed column was 9.85 ml, measured from the retention time of the peak of an iodine sample. The total porosity of the column is thus 0.720.

Fig. 3 shows the radial scans of grayscale intensity vs. normalized column radius for a packed column and for the same column, unpacked, both being filled with a 0.58 $g\,l^{-1}$ iodine solution. The radial scans were made approximately at the midpoint of the column axis. The two scans are similar. As expected, the grayscale intensity in the packed column was everywhere lower than in the empty column. However, the ratio of the absorbances measured at all radial positions was smaller than the porosity of the packed column. This required the determination of calibration curves for the packed columns, using the procedure described earlier in this section and inspired from frontal analysis.

The chromatographic process is usually accompanied by a serious dilution of the sample. A 12 $g\,l^{-1}$ solution injected in 20 μl samples was used in subsequent zone migration studies. The treated sam-

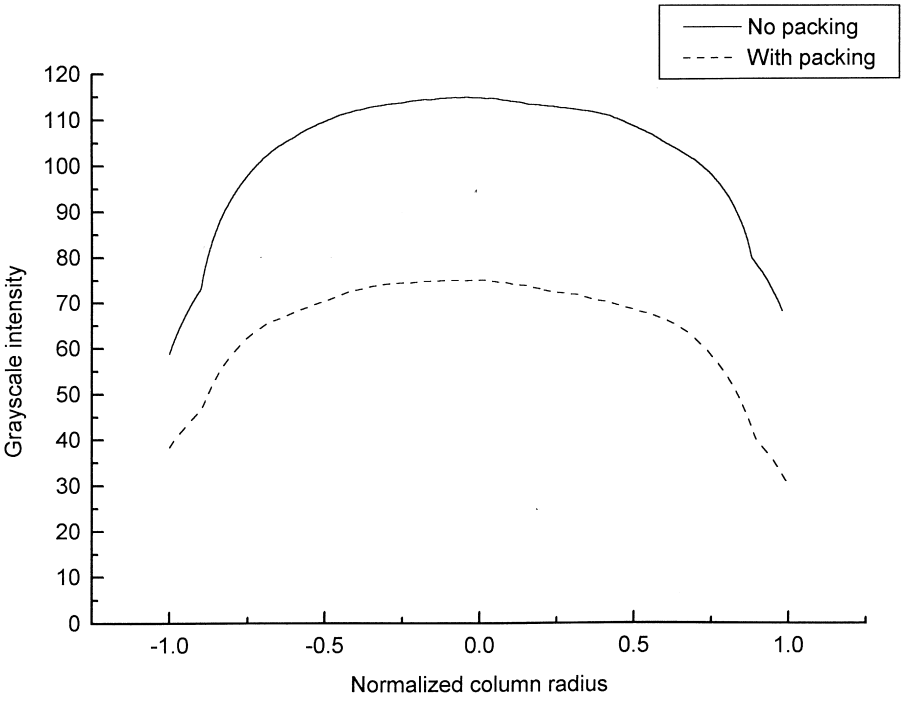

Fig. 3. Graph of the grayscale intensity vs. the normalized column radius for a 41-pixel-wide transverse scan at the midpoint of the packed column (dashed line) and the empty column (solid line).

ple images produced grayscale intensities no higher than 100. This value falls within the region of linear behavior of the calibration curve, from 0.10 g l^{-1} to 1.0 g l^{-1}, which was chosen as the concentration range for the calibration curves to be used for analysis. Fig. 4 shows the series of these calibration data corresponding to the left-hand side (LHS) of the column [Fig. 4(a)], including the center and the best-fit curve to the center data [Fig. 4(b)]. The differences between these curves are directly correlated with the differences in optical path length resulting from their different radial distances. The best-fit equation, different from Eq. (1), is:

$$C = e^{(a+b\sqrt{I})} \quad (2)$$

where C represents the concentration of iodine in g l^{-1}, I is the grayscale intensity, and a and b are numerical coefficients. The r^2 values for these correlations are all larger than 0.995.

Fig. 5 shows the digital image obtained before background subtraction for the zone of a 20-μl sample of 12 g l^{-1} iodine solution, 3.0 min after its injection. The grayscale intensity values measured from the digital image, at increasing distances along the column axis and at 0.1 increments of the column radius, starting from the center, were placed into a spreadsheet, making the application of Eq. (2) a relatively simple matter. The a and b coefficients were determined for each radial position and applied only to the grayscale values corresponding to that position in the digital image of the zone. As an example of the results obtained, Fig. 6 shows: (a) a height-normalized plot of the grayscale intensity vs. the migration distance along the center band of the column; (b) a height-normalized plot of the concentration vs. the migration distance using the empty column calibration method; and (c) a height-normalized plot of the concentration vs. the migration distance using the packed column calibration method. The corresponding post-column UV–Vis detector response is shown in Fig. 7. Note that the peak asymmetry in Fig. 7 is markedly stronger than in Fig. 6 and is in the opposite direction. The latter observation was expected since those concentrations which are further along the column in Fig. 6 are the first ones out of it in Fig. 7. The former will be explained later in this report.

3.2. Effect of the refraction of light

Refraction of light occurs due to the curvature of the glass column wall and the slight difference between the refractive indices of the solvents on both sides of the column wall and the glass wall. This results in a distortion of the apparent inner dimensions of the column [2]. Hence in order to establish the exact coordinates of the sample regions, the need for a correction to account for this refraction needs to be addressed.

In our initial report describing the process of solute visualization [2] we employed a carbon tetrachloride reservoir to assist in minimizing the cylindrical lens effect. Even so, some refraction would still occur due to the differences between the refractive indices of the glass (1.473) and the carbon tetrachloride (1.460). The application of Snell's law and some geometrical simplifications allows this effect to be evaluated with a suitable degree of confidence (see below). However, in the current study, we had to replace the carbon tetrachloride in the column reservoir with dichloromethane (1.424). This was done for three reasons, the primary one being consideration of occupational health and safety issues. Carbon tetrachloride is now considered as an extremely poisonous solvent, toxic to the human body in both the liquid form (dermal or oral contact) or the vapor phase (respiratory inhalation). Consequently, we sought to minimize contact in this long-term study. Columns and sample cells had to be frequently replaced, requiring them to be removed from or inserted into the reservoir. This was the most frequent and serious source of contact of the operator with the solvent. Secondly, carbon tetrachloride is an expensive solvent, which is now rather difficult to obtain. We recycle all our carbon tetrachloride, but even so, the reservoir volume is reasonably large and, over a period of time, we experienced a significant loss of solvent (evaporation to the hood). Thirdly, since the refractive index of dichloromethane is only slightly lower than that of carbon tetrachloride, this latter solvent appeared as an acceptable alternative.

We found that the refractive index of CH_2Cl_2 was not so low that the cylindrical lens effect is noticeable to the naked eye. Consequently, this was a reasonable solvent with which to evaluate whether a

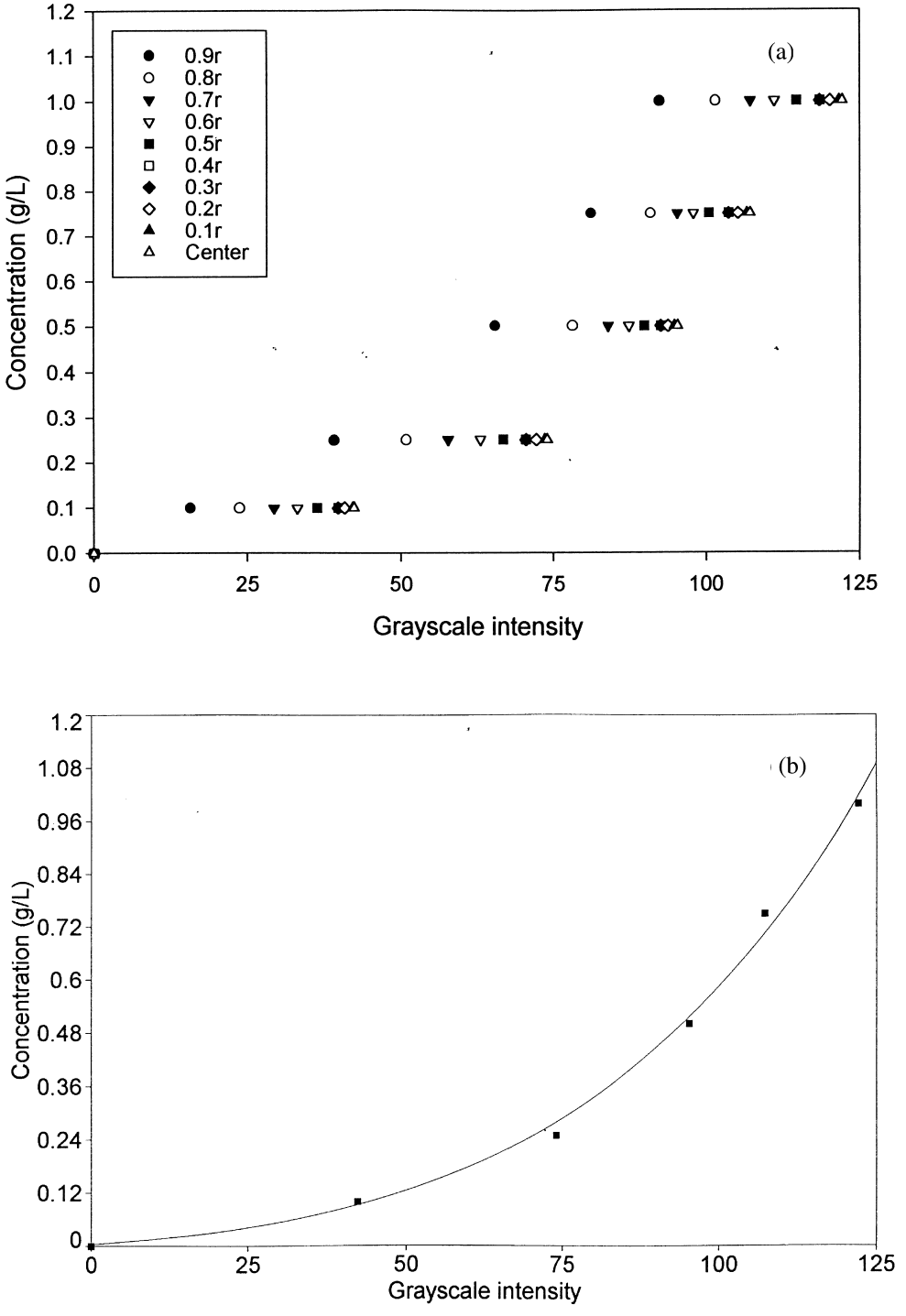

Fig. 4. Calibration curves in a packed column. (a) Calibration data for the nine bands on the left-hand side (LHS) of the column and in its center. Concentration range 0.10–1.0 g l^{-1}. (b) Calibration curve for the band in the column center.

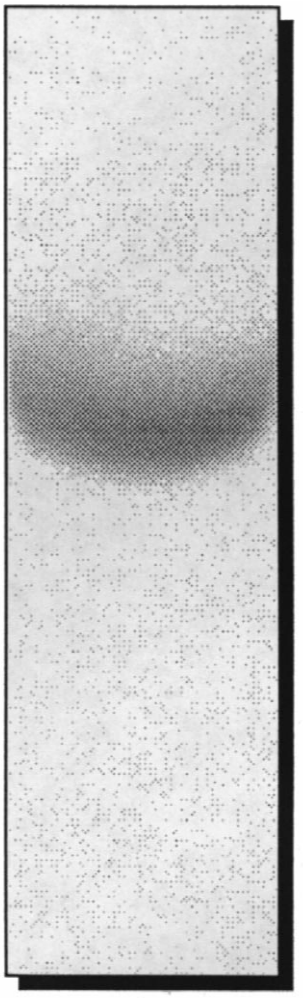

Fig. 5. Photograph of an iodine zone 3.0 min after injection. Injection volume, 20 μl of a 12 $g\,l^{-1}$ iodine solution in carbon tetrachloride. Flow-rate, 1.5 $ml\,min^{-1}$; shutter speed, $1/60\ s^{-1}$; aperture, f 16.

correction should be made to account for the refraction of light. Fig. 8 shows a light beam coming in the direction of the optical axis of the camera, at a radial distance d from the column and the camera axes. There is no refraction at the vertical glass walls of the reservoir. A light ray hits the first or external solvent–glass interface in M. The incidence angle of the light ray is i_4. This angle is related to the radial distance by:

$$d = (R + e) \sin i_4 \tag{3}$$

where R is the internal column radius, and e is the glass thickness. The angle of the refracted beam, i_3, is given by Snell's law as:

$$\sin i_3 = \frac{n_R}{n_G} \sin i_4 \tag{4}$$

where n_R and n_G are the refraction indices of the solvent in the reservoir and the glass, respectively. The refracted ray hits the second or internal glass–solvent interface in N'. Because the glass wall is thin and the three refraction indices are close, the distance of N' to the radius OM is small. As a first approximation, MN' is equal to the glass thickness, e, and $N'N$ (N is the intersection of OM and the inner glass–solvent interface) is perpendicular to OM. So, we have:

$$NN' = R \tan i_5 = e \tan i_3 \tag{5}$$

The incidence angle on this second interface is i_2 (Fig. 8). We observe now that, in the triangle OMN', the angle i_2 is equal to the sum $i_3 + i_5$ because these two angles have the same supplement (i.e. the angle $\angle ON'M$). The refraction angle, i_1, is again given by Snell's law and:

$$\sin i_1 = \frac{n_G}{n_C} \sin i_2 = \frac{n_G}{n_C} \sin(i_3 + i_5) \tag{6}$$

The radial distance of this light beam inside the column is:

$$d' = R \sin i_1 \tag{7}$$

The refracted light beam is parallel to the incident light beam if the angle i_1 is equal to the sum $i_4 + i_5$. If this condition is verified, then the same rational can be followed when the light ray exits the column, crossing the wall a second time. Then, the emerging light beam, collected by the camera is also parallel to the optical axis of the camera.

Numerical calculations using the numerical values pertaining to the experimental case discussed (R = 0.85 cm, e = 0.40 cm, n_R = 1.424, n_G = 1.473, n_C = 1.460) are easily carried out using a spreadsheet to perform the successive derivations as outlined above. The results obtained are illustrated in Fig. 9 which shows that the relative reduction of the width of the light beam is insignificant over most of the cross-section of the column. The effect is smaller than 5% for the center of the picture, i.e. $\pm 0.70R$. For the intermediate range, between $\pm 0.70R$ and $\pm 0.95R$, the effect is between 5 and 8%. Corrections for the

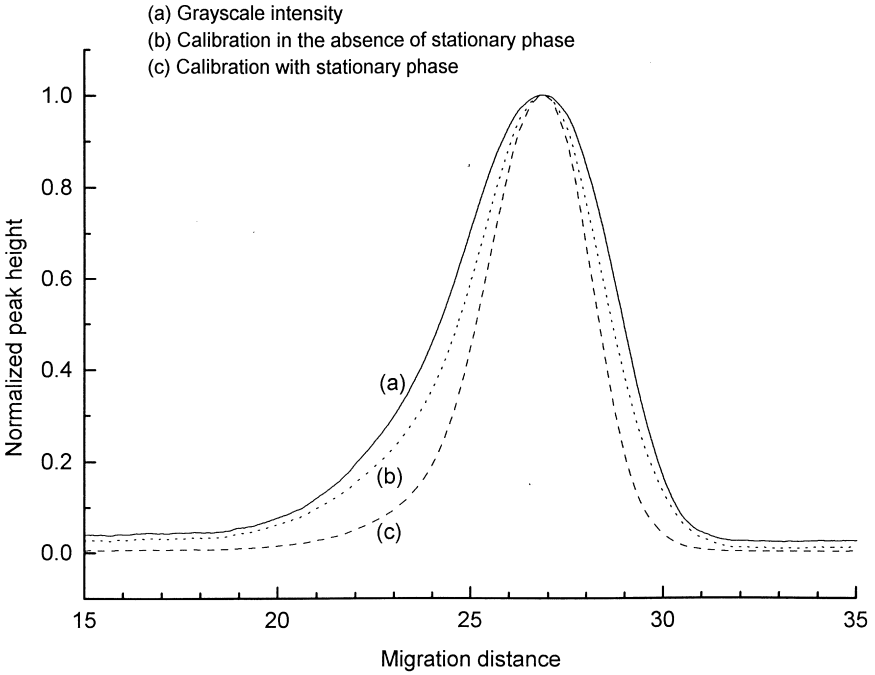

Fig. 6. Height-normalized grayscale intensity profile (a) obtained from scanning the grayscale density of the photograph in Fig. 5. Height-normalized concentration profile (b) derived from (a), following standardization of the intensity profile against the calibration curves in the absence of stationary phase. Height-normalized concentration profile (c) derived from (a), following standardization of the intensity profile against the calibration curves for the packed column as shown in Fig. 4.

refraction effect could easily be derived and applied, if needed since they are relatively small in comparison with the errors made (see later); however, this particular source of error is entirely negligible. Finally, the results of the calculations (not shown) give a residual $i_4 + i_5 - i_1$ which is extremely small, a few tenths of a degree in the center region, less than 0.7° close to the edge. The rays hitting the column in the direction parallel to the optical angle of the camera are transmitted through the column with a negligible scattering.

The same calculations can be carried out with different combinations of refractive indices, simulating different reservoir solvents, for example. In the column center, the refraction effect decreases with decreasing difference between the refraction angle of the solvent in the reservoir and that of the glass wall and tends toward 0. It would be completely negligible (less than 0.1%) with cyclohexanol ($n = 1.466$) over the central half of the column. However, the decrease which is observed closer to the column edge is less important and, there, the potential gain associated with replacing dichloromethane with cyclohexanol is insignificant.

Actually, at $0.9R$, the refraction resulted in a 20-pixel shift. As a result of this shift in radial location, the path length calculated at any location is slightly different from that derived from the size of the column cross-section and the radial location. The resulting effect on the peak shape, as a consequence of the light refraction, will be evaluated in the section detailing the analysis of the errors made in the visualization technique.

3.3. Normalization of the concentration distribution

Normalization is required when the concentration distribution of the sample across the chromatographic zone is sought. This step involves calculating the area of the column along each and any vertical column slice. The concentration distribution of the

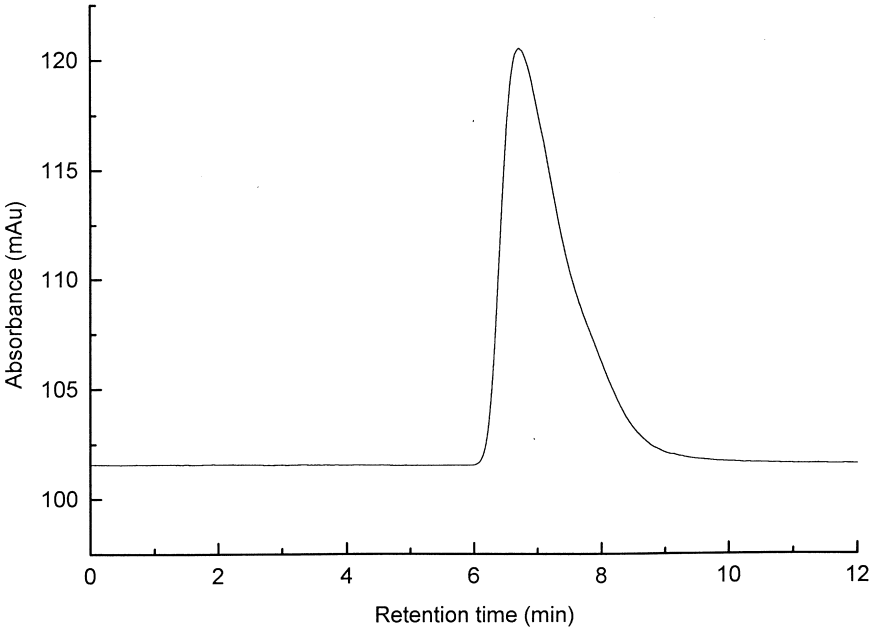

Fig. 7. Conventional chromatogram obtained with the post-column UV–Vis detector, for the iodine sample photographed in Fig. 5. Detection wavelength 440 nm.

sample zone is integrated between $l = 0$ and $l = L$, where L is the column length. The subsequent area under the curve is divided by the corresponding column section area.

4. Results and discussion

This section is concerned with the evaluation of concentration profiles of the zone inside the column, either in the axial or the transverse direction, and with the analysis of the reproducibility of the data obtained with this method. Because of the complexity of the procedure, the potential sources of errors are numerous. Their extent can be limited by proper operation, however, and some corrections can be made for the most important ones.

4.1. Concentration distributions

In the section detailing the calculation process of the concentration profile from the corresponding grayscale intensity profile, we compared the height-normalized zone profiles to illustrate the importance of accounting for the non-linear response of the detector (see Fig. 6). Using a calibration curve and a response factor for each radial location is equivalent to normalizing the concentration profiles to the corresponding volume of column bed examined. Once the response integrated over each bunch of pixel of the digital image is determined, the corresponding average concentration (averaged over the length of the optical path) is calculated. As long as the entire zone remains inside the column, the total area of the whole concentration distribution is constant and proportional to the sample size. (In this integration, the volume element is $f(d)\,dd\,dh$, with dd and dh the differential elements of transverse distance and column length, respectively, and $f(d)$ the length of the chord at a transverse distance d.) Concentration distribution in different regions indicate the distribution of the sample across the column.

To illustrate the importance of this result, we show in Fig. 10 plots of the local concentration of the zone along the axial direction for the 10 column bands [Fig. 1(a)] on the left-hand side (including the center slice) of the photograph shown in Fig. 5 [Fig. 10(a)] and for the 10 column sections on the right-hand side

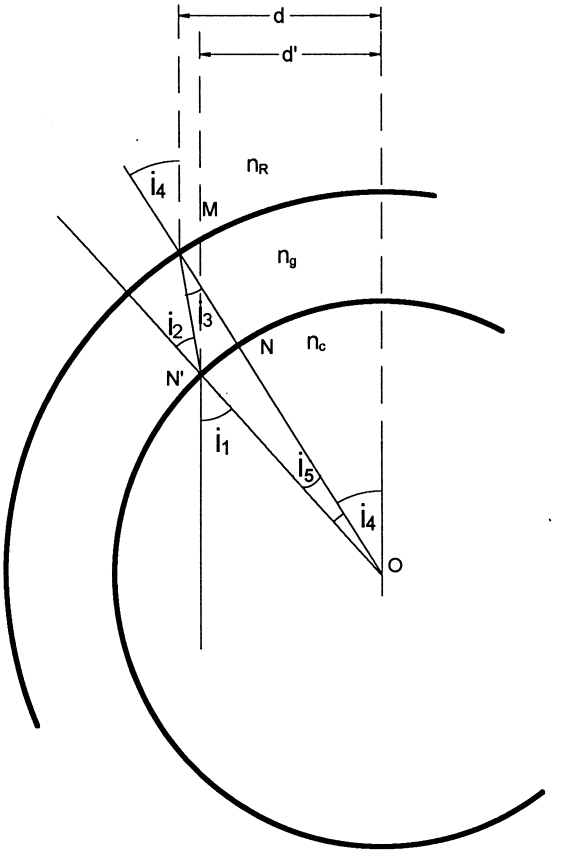

Fig. 8. Illustration of the refraction of light as it passes through the column and the sample reservoir (not to scale). See text for details.

[Fig. 10(b)]. The concentrations reported are derived from the calibration curves in Fig. 4. They are concentrations averaged across the column, along the direction of the optical axis of the cameras. These curves suggest that the local concentrations averaged along the different chords of a column cross-section are comparable, hence that the sample distribution at the column inlet was reasonably flat and homogeneous. However, important radial differences in mobile phase velocity and bed efficiency are visible.

From the profiles shown in Fig. 10, the area under each curve can be determined to yield plots of the peak area vs. the radial location as shown in Fig. 11(a). This figure shows that, in this experiment, the distribution of the sample concentration at injection was relatively homogeneous throughout the central region of the column but suggests that there was a slight decrease of this concentration toward the wall. The origin of the radial inhomogeneity of the injection is discussed in the companion paper [5]. It shows that the profile of the injected zone is not perfectly flat and that the inlet head fitting and frit do not always supply a rapid and uniform sample distribution. Frequently, the inlet profile turns out to be bowl-shaped, hollow in the center.

The concentration profiles shown in Fig. 10 were not corrected for the refraction of light. Applying the refractive index (RI) correction factor discussed in the experimental section (see Fig. 8), which corrects for the shift between the true radial location and the apparent radial location, we obtained a corrected radial distribution profile which overlays nearly exactly the uncorrected profile in Fig. 11 for all bands within $\pm 0.7R$. Differences become significant near the wall, where light refraction is due to the curvature of the glass wall, hence radial shifts are the most important. Deviations larger than 5% could occur only at radial distances in excess of $0.7R$. At $0.9R$, however, a 1% difference only was found between the corrected and uncorrected peak areas. Although this may limit the extent of certain conclusions, this observation does not reduce the interest of the determination.

The derivation of the local column efficiencies from the axial concentration profiles showed that no discernible difference was observed following the application of the refractive index correction, except close to the column edge (Fig. 12). Reduced plate heights were measured using both the variance method [2] and the peak-width at half-height method. Likewise, little changes in the migration distance (location of the peak maximum) were observed (Fig. 13). This result was expected since the correction is small nearly everywhere and since it has no axial component.

During the process of zone analysis, the profile is sectioned into transverse slices in the depth direction (i.e. parallel to the camera axis), as shown in Fig. 1. In general, there are 19 slices at intervals of $0.1R$. Each slice was equivalent to between 41 and 43 pixels wide (or 0.8355 mm). Sectioning the image is a tedious and time-consuming process, particularly if a high precision of the section slice is to be maintained. The results derived from the theoretical and experimental discussion made on the influence of

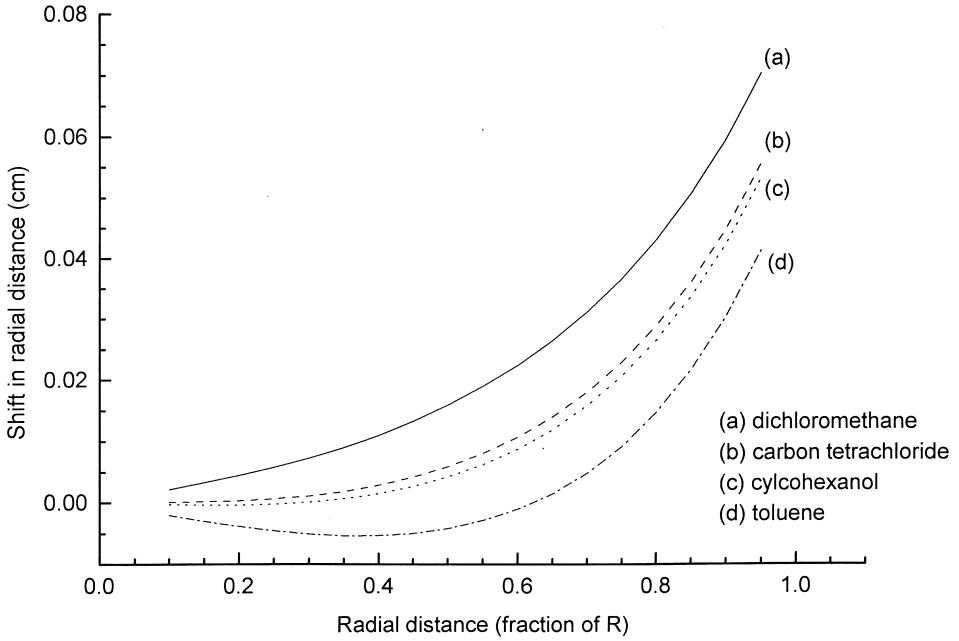

Fig. 9. Influence of the refraction angle on the apparent width of the column. (a) $n_R = 1.424$; (b) $n_R = 1.466$; (c) $n_R = 1.464$; (d) $n_R = 1.496$.

refraction and the change in length of the optical path allow the determination of the degree of precision required for this process. To answer this question we deliberately offset the column sectioning by 10 pixels (i.e. 0.1943 mm) to the right-hand side. This is a large error that far exceeds the normal limits of precision. Even so, when the concentration distributions of the corresponding zone sections were calculated, there was no significant change in the peak area ($< 7\%$ at $0.8R$), the column efficiency or the migration distance. For example, the plot of the peak area vs. the radial location for two analyses made from the slices separated by 10 pixels are shown in Fig. 14. The data overlay almost exactly, except at the edges. Consequently, a tolerance of more than a few pixels is afforded in the subdivision of the column into vertical slices.

4.2. Repeatability and reproducibility of the results

An important aspect of the applicability of this method of quantitative investigation of the column properties through visualization is the degree of reproducibility of the data obtained. In studying this reproducibility, several aspects must be considered, namely: (1) the reproducibility of the quantitative data obtained with the slide scanner — both from slide to slide and from day to day; (2) the reproducibility of these data from slide to slide within one roll of film; and (3) their reproducibility between different rolls of film.

4.2.1. Reproducibility of the slide scanner

One slide was scanned a total of 12 times, three times successively at intervals corresponding to 3 min, 30 min, 90 min and 240 min after the scanner was initialized. The process was repeated on a second day. The corresponding intensity profiles are shown in Fig. 15. The mean peak area was 474.19 (arbitrary units) with a relative standard deviation of 4.4%. The overlay of these profiles is almost perfect, and, clearly, the day-to-day variation in the performance of the slide scanner is small. This study of the slide scanning process also takes into account the process of background subtraction, an operation which is done on each slide, immediately after acquisition of the digital image [2].

4.2.2. Reproducibility from one slide to another

To test for slide-to-slide variations, triplicate in-

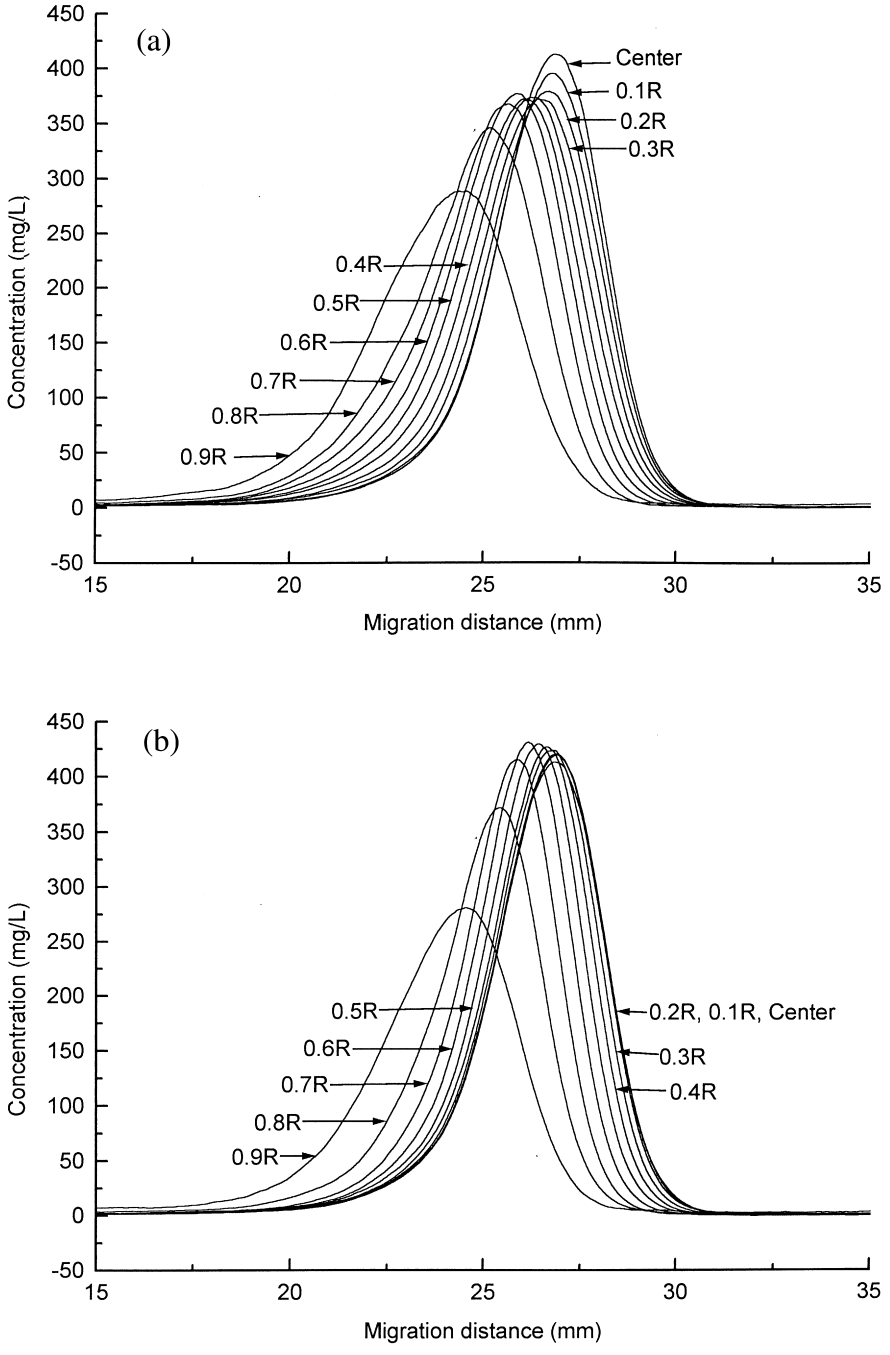

Fig. 10. Comparison between the axial concentration profiles along the different vertical bands derived from the photograph shown in Fig. 5. (a) Profiles for the nine column sections on the left-hand side and the center section. (b) Profiles for the nine column sections on the right-hand side and the center section.

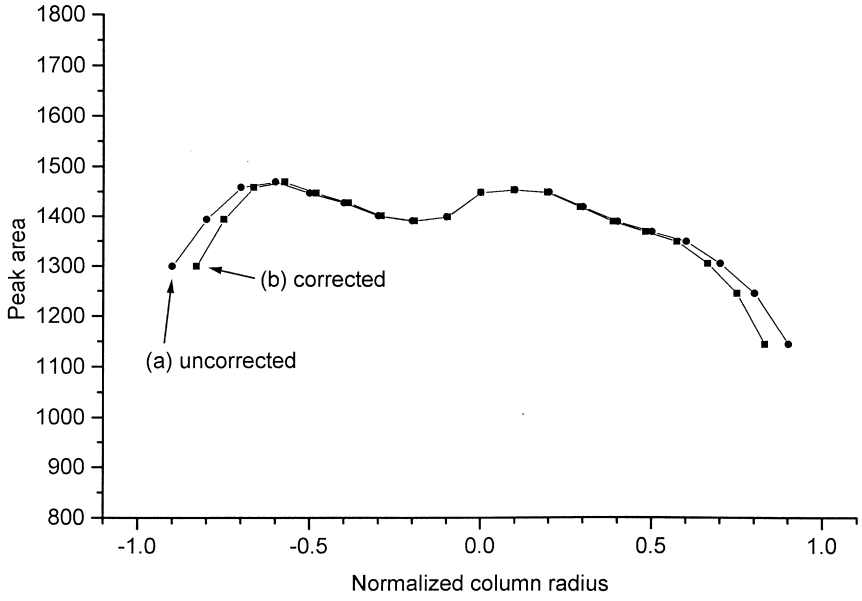

Fig. 11. Peak area vs. the radial location. Plot derived from the concentration profiles in Fig. 10. (a) Areas measured from uncorrected zone profiles. (b) Areas measured from refractive-index corrected zone profiles.

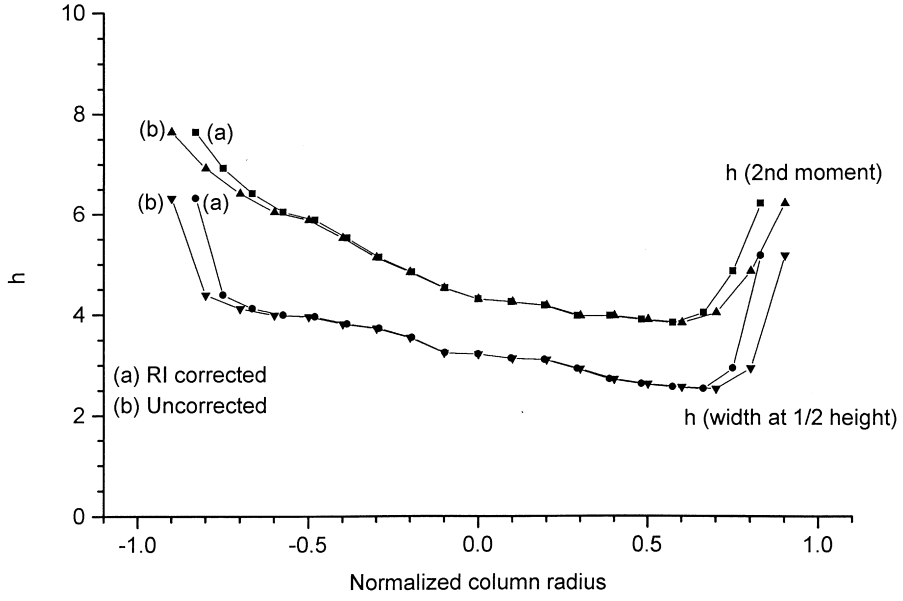

Fig. 12. Column efficiency vs. the radial location. Plots derived from the concentration profiles corrected and uncorrected for the influence of the refractive index. *h* values were measured from the second moment and from the peak-width at half-height.

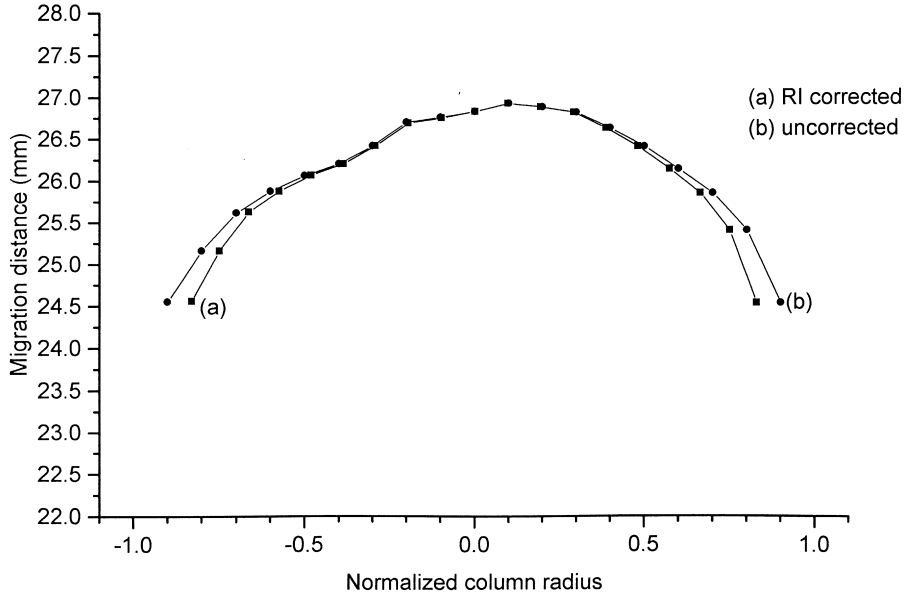

Fig. 13. Migration distance vs. radial location. Plots of the solute migration distance (measured from the peak maxima) derived from the profiles in Fig. 10, before and after correction for the influence of the refractive index.

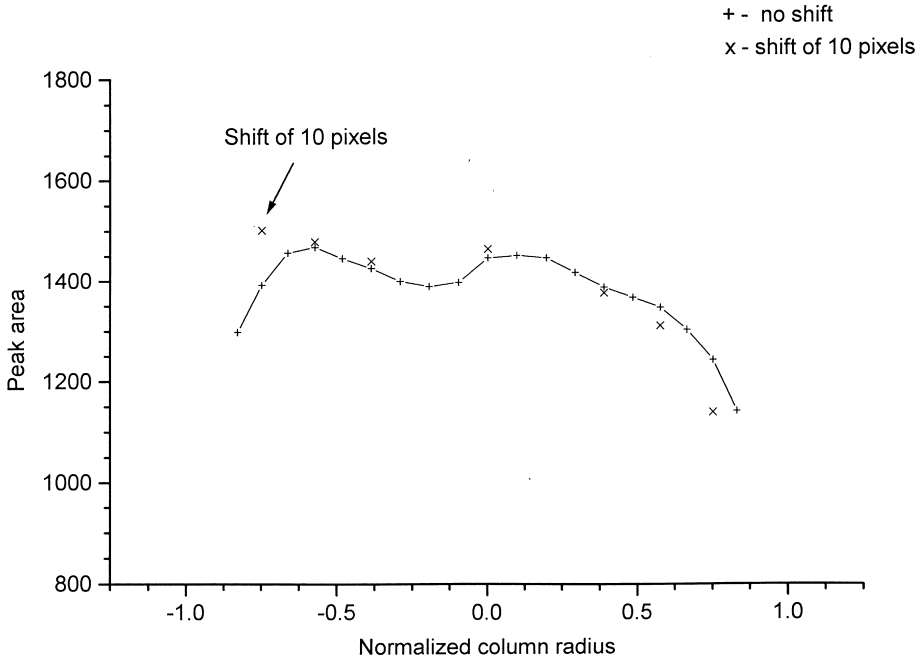

Fig. 14. Effect of an inaccurate division of the digital image of the zone into vertical bands. The vertical bands were deliberately offset by 10 pixels to the right, equivalent to 0.1943 mm.

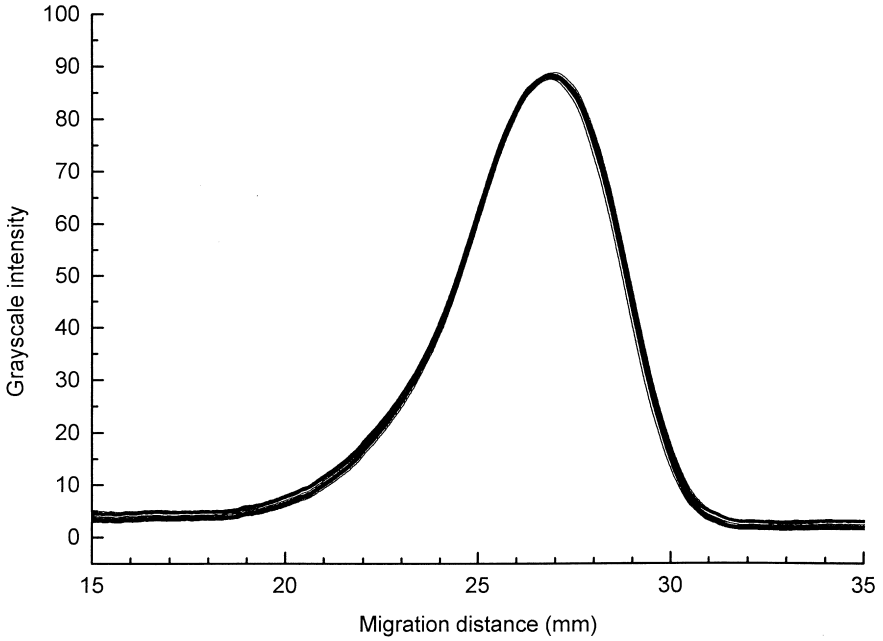

Fig. 15. Reproducibility of the slide scanner. A total of 24 scans were made over a period of 2 days. The area reproducibility was better than 5% RSD.

jections of the iodine sample were analyzed. Thus, the reproducibility data below include the contribution of the sample size repeatability. The corresponding migration profiles were processed according to the details just described and each migration zone was divided into 19 vertical slices. Following correction and normalization of the axial concentration profiles, their peak area, migration distance, and column efficiency were measured and compared. Fig. 16 illustrates the reproducibility of the peak areas as a function of the radial location. In all cases, the degree of reproducibility was high (the range for the three measurements was 9% of the mean in the worst case, which again was closest to the wall). Likewise, the retention times for each sample overlaid almost perfectly as shown in Fig. 17 (the range for the three measurements was 0.6% of the mean in the worst case). Long-term experience with this system showed that significant deviations of the retention times are most probably caused by fluctuations of the flow-rate delivered by the pumping device.

A good agreement was also observed for the replication of the reduced plate heights (Fig. 18). The reproducibility was higher for the half-height method than for the variance method, but even then the range of the results of the three measurements was less than 20% in the worst case, when using the second moment. Clearly, slide-to-slide variations were small. We should note, however, that for one of the slides only half the column could be analyzed, due to a water mark that stained permanently the surface of the slide. This mark was an accidental result of the developing process. Such stains are rare, but their presence does emphasize the degree to which the slides should be cared for in order to avoid such contamination. We note also that, occasionally, an artifactual hump is observed on a concentration profile [4]. The presence of such artifacts was too infrequent to allow the determination of their origin (possibly the development process).

4.2.3. Reproducibility of different rolls of film

Film-to-film variations were tested by analyzing triplicate injections of the same iodine sample as done above. The experiment was carried out in exactly the same manner as previously, with a single roll of film, but a new roll of film was used. The

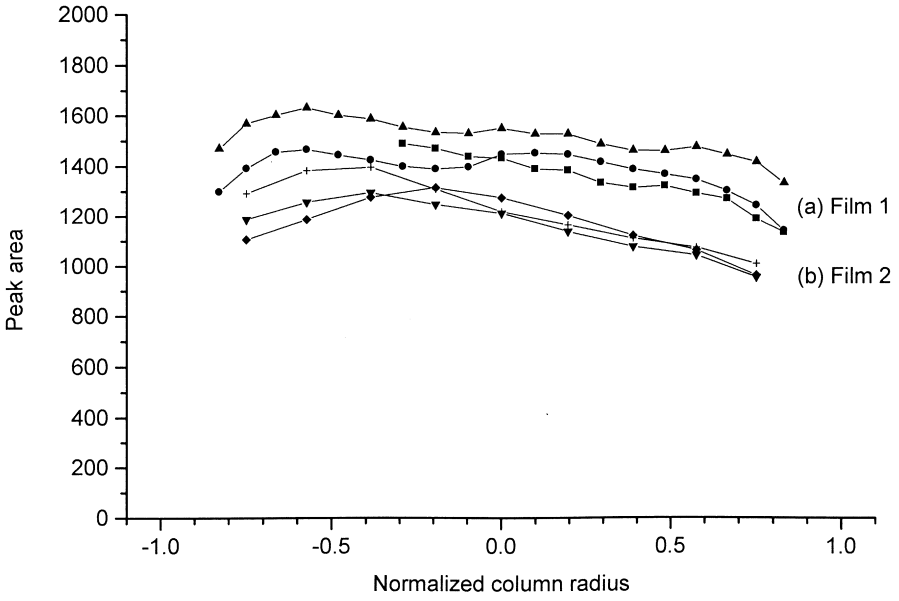

Fig. 16. Reproducibility of the normalized peak areas. Results of triplicate injections of the iodine sample. The test was performed over 2 days and on two different rolls of film. (a) Film 1. (b) Film 2. Note that only every second data point was plotted on (b).

image was photographed 3 min after the injection. In these tests, however, the image was divided into nine sections instead of the 19 sections, the width of each section remaining the same as that used for the first roll of film.

The results in Fig. 16 show that there were minor

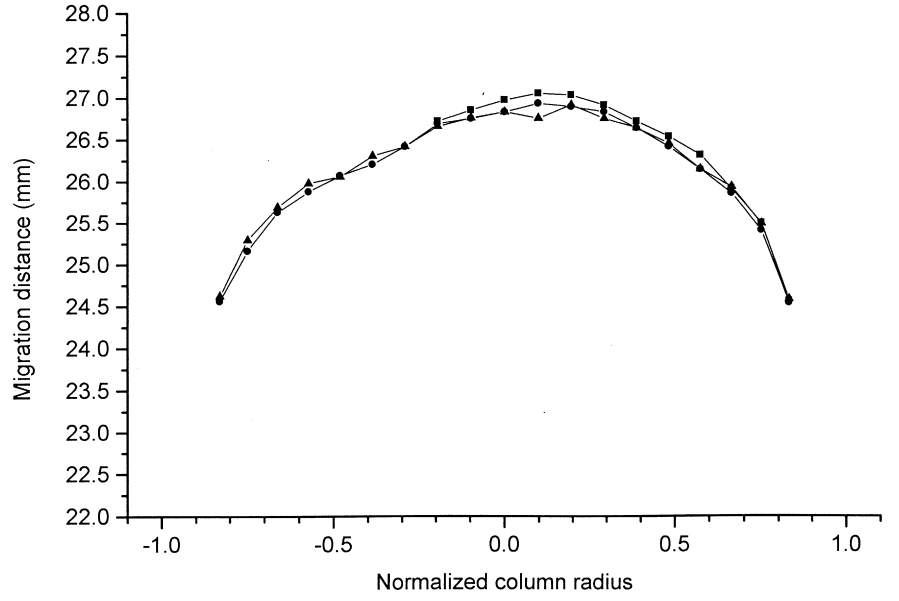

Fig. 17. Reproducibility of the migration distance for triplicate injections of the iodine sample.

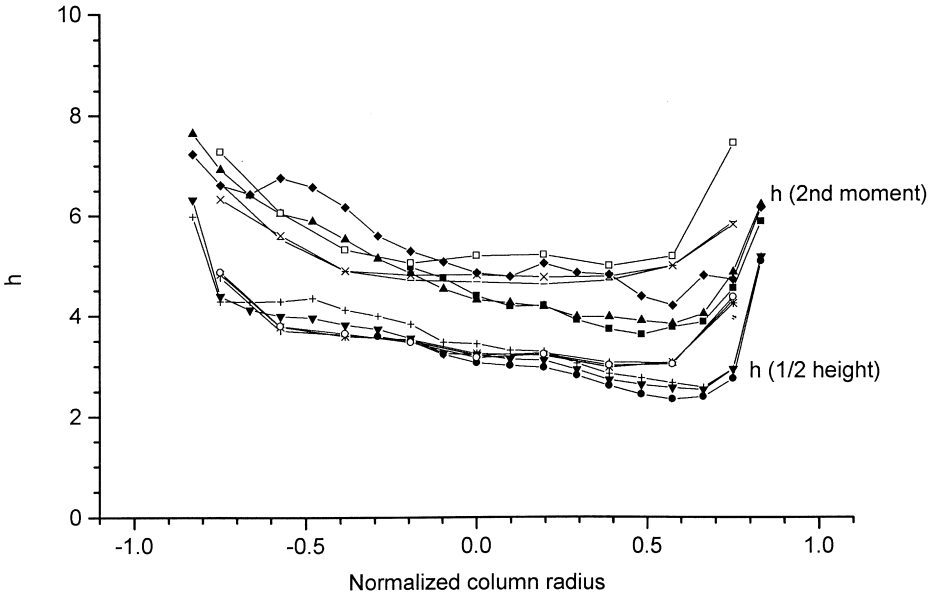

Fig. 18. Reproducibility of the column efficiency for triplicate injections of the iodine sample, performed on two different films, at 2-days distance.

differences between the areas of the concentration profiles measured in the same column location with either roll of film. At 0.8*R*, the region of poorest reproducibility, the difference between the means was 24%, while in the center of the column it was less than 16%. For much of the column, the reproducibility of the peak efficiency remained almost unchanged. However, there were some discernible differences, which need to be commented on, as shown by a comparison of the curves in Fig. 18. The results for Film 2 showed that the column was more homogeneous and symmetrical than when tested using Film 1. The efficiency on the left-hand side of the column had improved to the level of that on the right-hand side. Part of or all the explanation arises from the fact that this column was prepared 2 weeks prior to this particular experiment and that 3 days elapsed between the exposures of Film 1 and Film 2. We believe that this result does not reflect an error in the quantitative result due to some differences between the film properties, but rather highlights the fine discrimination that is possible when using this on-column technique. The column had experienced some further consolidation in the mean time and its properties had slightly evolved. The conventional post-column UV–Vis detector responses confirm a slight improvement in efficiency for the samples injected and recorded on the second roll of film. The efficiency improved from $h = 18.6$ to $h = 17.2$ (based on h obtained from the second moment). Close inspection of the photographs revealed that on Film 1 there was a hump in the tailing edge on the left-hand side of the sample zone. This hump was no longer present in the photographs on Film 2. However, these visual differences between the images of the two zones, while faintly noticeable when compared side by side on a computer monitor, do not translate well to a hard copy, thus they are not shown here. Such a result may also be due to irregularities in the injection, or possibly to a change in homogeneity of the inlet frit, which is the subject of the companion paper [4].

4.3. Comparison to conventional post-column detector response

Standard UV–Vis post-column detection (440 nm) of the iodine sample zones showed that the reproducibility of the peak area for triplicate injections was 1.1%. This was similar to the reproducibility of

the peak areas obtained with the 'on-column' method for the region of the column between $\pm 0.7R$. The efficiency of the concentration profiles given by on-column detection is much higher than that of the elution profiles (Fig. 20). The reduced plate height of the column determined from the second moment using the post-column UV–Vis detector was $h = 18$ with a relative standard deviation of $\pm 2\%$. Obviously, this is in poor agreement with the results of the on-column measurements. This low efficiency was not surprising. First, the migration distance after a given development time varies markedly with the radial position (Fig. 17). Second, the width of the peaks recorded in post-column detection is influenced by the extra-column sources of zone broadening (e.g. exit tubes, peripheral fittings, and frits after the column, including the detector flow cell). In a companion study [5], we examine the effects of the inlet fitting. The results obtained are much more detailed and complex than what most chromatographers would have previously acknowledged. However, no attempts were made in this first study to investigate the contributions of the outlet fitting although previous work showed this to be a source of flow distortion [3].

Fig. 19 compares the zone profile obtained by post-column UV–Vis detection to the zone profile taken from the central section of the sample zone, using on-column photographic detection. The on-column profiles show that a slight degree of tailing resulted during the migration along the bed. The post-column detector showed a much more severe tailing. This additional tailing originates in part in the extra-column volumes, but also in the design of the outlet fitting. In addition, the post-column detector is a bulk detection device. It sees the entire zone. A more relevant comparison between the on-column migration profile and the post-column detector elution profile may be obtained by summing the individual concentration profiles of each vertical section in proportion to their respective cross-section area. The overlay of the migration profiles shown in Fig. 10 and the variation in migration distance as a function of the column radius (Fig. 13) should lead

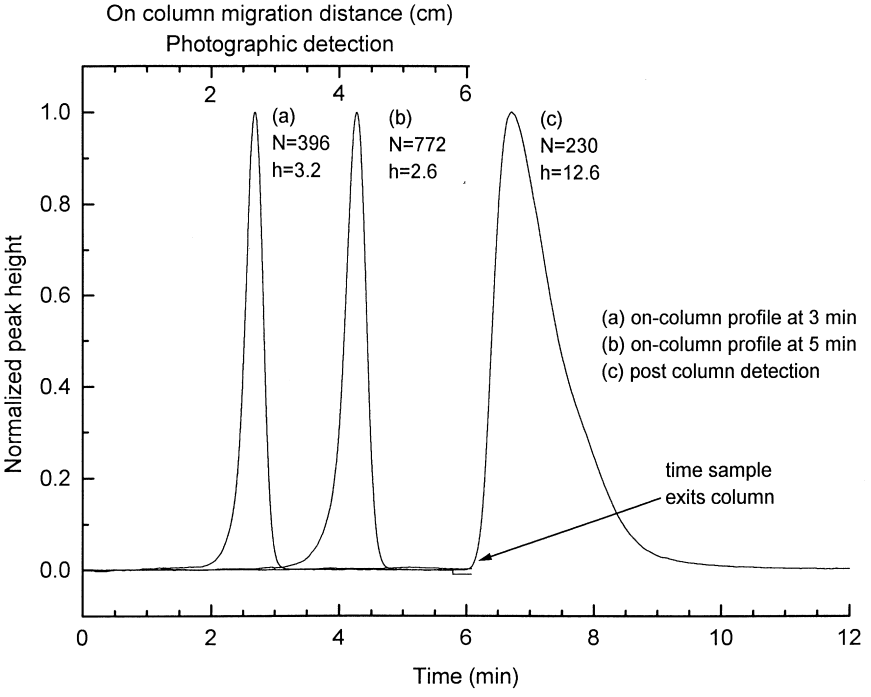

Fig. 19. Comparison between the height-normalized on-column detection zone profiles and the height-normalized post-column detection zone profile of an iodine sample zone. Flow-rate, 1.5 ml min^{-1}. The sample exits the column at approximately 6 min.

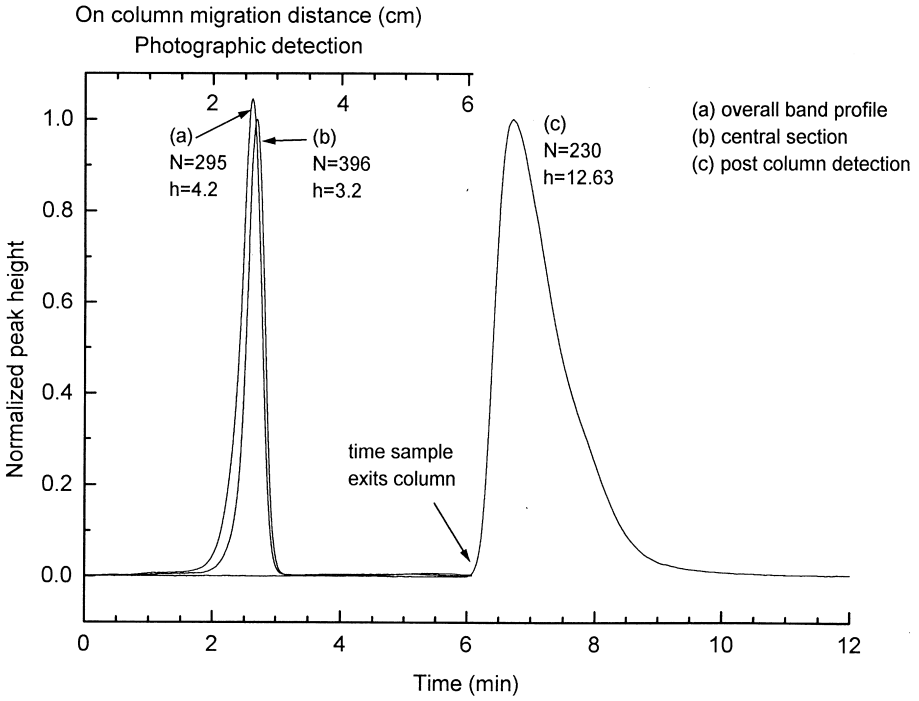

Fig. 20. Comparison between the height-normalized on-column detection zone profile, the height-normalized on-column detection zone profile obtained from the summation of 19 sections and the height-normalized post-column detection zone profile of an iodine sample zone. Flow-rate, 1.5 ml min^{-1}. Retention time of iodine, approximately 6 min.

to peak tailing. In fact, the zone profile showed only a slight increase in the tailing and a small change in the location of the peak maxima, as shown in Fig. 20. This confirms the importance of the exit fitting to which less attention is often paid.

5. Conclusion

This study showed that quantitative information can be obtained from photographs of chromatographic zones taken on-column, during their migration. Successful quantitation necessitates that these photographic images be of a high quality. Cleanliness of the column wall, the reservoir walls, and the resulting slides is of the utmost importance. Manufacturers of film recommend that professional film be used for the highest degree of color density reproducibility. We did and experienced no problems there. Once a suitable image is collected, quantitation involves first the conversion of the photographic image to a digital image, grayscale conversion, and background subtraction. In order to obtain concentration distributions, the density of the resulting image must be standardized against a calibration curve. To minimize the cylindrical lens effect, the column must be submersed in a solvent with a refractive index close to that of the stationary phase, the column wall, and the mobile phase. Some tolerance can be afforded in this respect, but if the region near the wall (the area of greatest refraction) is to be investigated, a correction for the refraction of the light beam must be made. In most cases, a central region extending to $\pm 0.7R$ of the column can be investigated with no correction and a resulting accuracy better than 7%, even when the refractive indices differ by as much as 0.05.

The reproducibility of the whole process was satisfactory, as shown by the results obtained with photographs of zone profiles obtained with triplicate injections, on different days, using different rolls of film. The slide-to-slide variations on the same roll of

film were small, with a maximum deviation in peak area of 9%, part of it due to the contribution of the slide scanner precision (4.4%). The reproducibility of the column efficiency was, in the worst case, 20% when determining N from the second moment. This error should decrease for solute zones that migrate further along the column bed and are wider. Reproducibility from one roll of film to another was also good, with differences in peak areas being in the order of 24% near the wall ($0.8R$) and less than 16% in the central region of the column.

Finally, we should note that this analysis was performed on a column having a relatively poor efficiency. The zones observed exhibited a rather severe degree of tailing. Accordingly, detection of the low concentrations in the peak tail is difficult because of the high limit of detection. As a result of this, the error in the measurement of the efficiency determined from the variance of the zone is higher than it would be for a more efficient column. By contrast, the values of N derived from the width at half-height exhibited less variation. We can expect that improvements in the column performance would also reflect upon improvements in the data precision.

Acknowledgements

This work was supported in part by Grant DE-FG05-88ER13859 of the US Department of Energy and by the cooperative agreement between the University of Tennessee and the Oak Ridge National Laboratory.

References

[1] B.S. Broyles, R.A. Shalliker, D.E. Cherrak, G. Guiochon, J. Chromatogr. A 822 (1998) 173.
[2] R.A. Shalliker, B.S. Broyles, G. Guiochon, J. Chromatogr. A 822 (1998) 173.
[3] R.A. Shalliker, B.S. Broyles, G. Guiochon, Amer. Lab. 30 (21) (1998) 124.
[4] B.S. Broyles, R.A. Shalliker, G. Guiochon, J. Chromatogr. A 855 (1999) 357.
[5] B.S. Broyles, R.A. Shalliker, G. Guiochon, submitted for publication.